Innovative Infrastructure Solutions (2024) 9:15
https://doi.org/10.1007/s41062-023-01316-1

TECHNICAL PAPER

Influence of concrete type on rigid pavement behavior under static loads

Magdy I. Salama[1] · Amal Elayat[1] · Mahmoud Reda[1] · Galal Elsamak[1,2]

Received: 23 August 2023 / Accepted: 22 November 2023 / Published online: 18 December 2023

Abstract
It is thought that rigid pavements are more expensive than flexible pavements. However, when taking into account the element of durability, it was found that rigid pavements are less expensive than flexible pavements and have a service life up to 20 years. The flexible pavements are more suitable for the areas with weak subsoil and poor drainage, but it has a negative impact on the environment. This research presents an experimental and numerical study to explore the behavior of rigid pavement made of different types of concrete under the influence of static loads. The recent experimental study consists of six slabs with dimensions of 600 × 600 × 60 mm made of different types of concrete. Such types are normal-strength concrete (NSC), high-strength concrete (HSC) and strain hardening cementitious composites (SHCC). Based on the findings of this study, it is evident that the slab constructed with SHCC exhibits a 76.6% greater bearing capacity compared to the NSC slab. Regarding cost-effectiveness, the HSC slab was identified as the most economically advantageous option. A point to be noted is that the numerical model using the Abaqus program succeeded in modeling the experimental tested slabs.

Keywords Concrete rigid pavement · Normal-strength concrete · High-strength concrete · Strain hardening cementitious composites · Abaqus

Introduction

The pavement is considered the link between the vehicle loads on the road and the foundation layers. A point to be noted is that the bearing capacity of the foundation layers is not taken into account when choosing the optimal path for the road. Therefore, the search for a type of pavement that can withstand high traffic loads and has the ability to resist the resulting subsidence in the foundation layers becomes a must [1, 2]. The road user needs appropriate means of comfort and safety on an ongoing basis. Such means need efficient pavement able to bear the repeated loads imposed by traffic and harsh environmental conditions, which may lead to irreversible deformations in the body of the road [3, 4]. To make a durable pavement, the surface layer must have the basic elements necessary to achieve such durability. Such elements are provided by using a water-impermeable layer. An important point to be noted is that water leakage through cracks and holes may lead to a change in the quality of the foundation layers and reduce the bearing capacity of the pavement [5, 6]. The pavement can be divided into two types according to the composition of the material used in the surface layer. Such types are the flexible pavement and the rigid pavement. Another point to be noted is that the foundation layers in both types are usually composed of materials with high capacity to achieve stability and endurance. With the use of such efficient materials, the traffic remains open during the paving process. Moreover, this traffic helps to generate loads, which increase the compaction of the foundation layers and reduce the cost of using compaction equipment. Furthermore, the traffic improves the bearing capacity of the foundation layers [7, 8]. The mechanical properties and durability of the road surface are equally important to provide the necessary resistance to avoid damage to the road. In addition, such properties increase the durability of the concrete and its resistance to the cracks. Furthermore, these properties reduce the pores, which in turn prevent the penetration of water and chemicals, such as acids, chlorides and sulfates to the foundation layers [2, 9,

✉ Galal Elsamak
jalaal_elSammak123@eng.kfs.edu.eg

[1] Department of Civil Engineering, Faculty of Engineering, Kafrelsheikh University, Kafrelsheikh, Egypt

[2] Department of Civil Engineering, Delta Higher Institute for Engineering & Technology, Talkha, Egypt

10]. Rigid pavements usually have a service life of 30–40 years. During this period, the integrity of the pavement structure must be maintained. A point to be noted is that the surface of these pavements is often treated throughout their service life to restore their efficiency. According to the highway code [11], crack widths in concrete pavement can be classified into three categories: narrow cracks of 0.5 mm width capable of fully transferring the load; medium cracks from 0.5 to 1.5 mm capable of partially transferring loads; and large cracks with a width of more than 1.5 mm that are not able to transfer loads.

Surface layer material is the basic criterion for road classification [2, 9, 10]. Asphalt materials are used in flexible pavement, and they are also called 'asphalt pavement' [12]. Unlike concrete pavements, asphalt pavements do not need joints and breaks to face the movement of expansion and contraction resulting from temperature changes. To handle this expansion and contraction in the pavement, which causes a degree of deformation, each road has a maximum degree of deformation that can be restored [13, 14]; unlike asphalt pavement, the concrete pavement requires longer time to be opened to traffic because concrete needs time to reach sufficient strength before being used [7, 12, 15]. It is worth mentioning that there is a type of a pavement called 'semi-rigid' or 'composite pavements,' which is a mixture of asphalt layers and recycled concrete. This type of pavements is made of high-quality asphalt and recycled concrete of lower quality. Therefore, it has both the strong bearing capacity of the rigid pavement and the advantages of the flexible pavement [16–20]. Numerous studies have examined the behavior of rigid pavements [21–29]. By using a small percentage of the recycled concrete, cracking may occur, and the pavement will begin to show early signs of collapse [2, 6, 30]. A point to be noted is that the rigid pavement or the concrete pavement usually consists of two layers: the foundation layers and the surface layer, which consists of the concrete slab. These slabs act as a basic support that strengthens the pavement. Furthermore, the slabs are placed on the high- and low-quality foundation layers [31, 32]. The use of a strong layer of concrete as a surface layer leads to the use of materials with a lower cost to be used as a filler layer over the weak base layer. This is because this slab works to improve the lower layer and increase its hardness [11, 32]. The higher the percentage of the cracks in the surface layer, the greater the possibility of dust and debris to go into the cracks. Moreover, these cracks allow the penetration of water into the foundation layers, which leads to the rapid deterioration of this layer. It is worth mentioning that the use of a low-strength concrete is one of the most important reasons that lead to such cracks [31, 33].

According to the authors' review of previous studies, as partially discussed earlier, it becomes evident that there are deficiencies in studying and comparing the impact of using different types of concrete on the behavior of rigid pavement. Therefore, the aim of this research is to investigate the influence of employing various concrete types on the behavior of rigid pavement, both experimentally and numerically, and to compare them in two aspects: strength and cost.

Experimental program

Materials properties

In the case of rigid pavement over weak subsoil, the primary factor in resisting external loads depends on the behavior of the concrete pavement used. Therefore, it is essential to study the behavior of rigid pavements made from various types of concrete.

To study the behavior of the rigid pavement made of different types of concrete, six concrete slabs with dimension 600*600*60 mm were prepared tested and divided into three groups. In addition, each group consisting of two slabs represents one of the following types of concrete: NSC, HSC and SHCC. Table 1 shows the quantities in kg to prepare cubic meters of each type. The design of the mixtures was based on the mixtures proposed by Elsamak et al. [34].

Two cylinders of size 150 × 300 mm were casted from each type of the concrete to be tested under compression. The compressive strength after 28 days was 31, 72 and 121 N/mm^2 for NSC, HSC and SHCC, respectively. Furthermore, two samples of each type of the concrete were prepared to be tested under direct tension. A point to be noted is that the tests of the two samples were made according to tests made by Zeng et al. [35] The tensile strength was 2, 2.25, 6 N/mm^2 for NSC, HSC and SHCC, respectively.

Table 1 Quantities in kg for the preparation of cubic meters of each type of concrete used

Type	Cement	Fly ash	Silica fume	Sand	Crushed basalt	Fibers*	Water	Super plasticizer**
NSC	332	–	–	662	830	–	206	–
HSC	460	80	54	600	980	–	130.7	9.2
SHCC	1300	–	230	146	–	15	297	30

*Polypropylene fiber consists of fibers 25 μm in diameter and 12 mm in length

**CMB Addicrete BVS

To study the behavior of the aforementioned slabs as rigid pavement layers above the base and sub-base layers, three different soil samples were used from a nearby site. Such soil samples were used as a sub-base layer. The basalt fracture was used from one of the local quarries as a base layer upon which the slabs were placed. A sieve analysis test was conducted on it, revealing that its maximum nominal size is 7 mm. The particle size distribution curve is depicted in Fig. 1. The following tests were carried out on each of the previous samples: granular gradient, modified proctor, CBR, degree of absorption of aggregates, degree of disintegration in water, Los Angeles and California borders. Furthermore, these tests were performed according to tests made by AASHTO [36]. The results of the tests are shown in Tables 2 and 3. The experimental study was conducted using the second sample shown in Table 2.

Test setup

To conduct the test, a unidirectional steel frame was prepared with a steel tank with a net dimension of 1000 × 1000 × 600 mm and a loading cylinder with a capacity of 500 kN in addition to a hydraulic pump. To calculate the settlement resulting from loading, the device was equipped with a displacement gauge with a 100-mm stroke. Figure 2 shows the main components of the device.

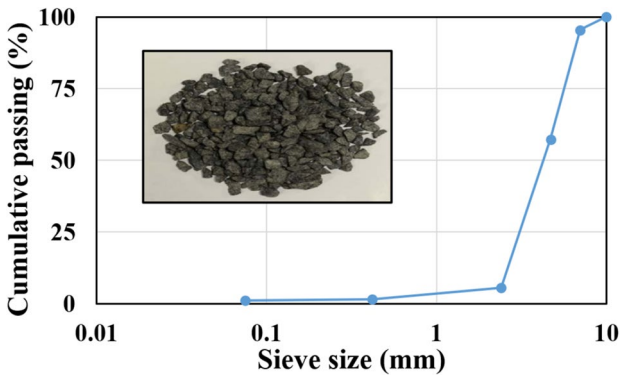

Fig. 1 Particle size distribution curve of the basalt fracture used as a base layer

Table 3 Results of the tests carried out on the aggregate used as a base layer

Test	Results	Specification
Water absorption	2.22%	Max. 10%
Disintegration in water	1.57%	Max. 5%
Loss Angeles	30.8%	Max. 40%
Modified proctor	Maximum dry density (g/cm^3) = 2.253 Optimum moisture content = 6.75%	
CBR	97.2%	Min. 80%

Three hundred millimeters of the sub-base was laid on two layers with a thickness of 150 mm for each one. Moreover, the necessary compaction operations were carried out on each layer using a reciprocating vibrator, which was sprayed with the optimum moisture content. After the completion of the compaction process, the sand cone test was performed. The result of the compaction rate was as follows: the first layer was 92%, while the second layer was 94%. It was worth mentioning that the base layer was placed on two layers with a thickness of 100 mm for each one. This test was performed in the same way as the previous test. The results of the sand cone test were as follows: the first layer was 97.5%, while the second layer was 98.5%.

After the completion of the compaction process, the MCO layer was sprayed at a spray rate of 1.5 kg/m^2. Moreover, the aforementioned slabs were placed on the top of the impregnation layer after using the final quick setting grout mortar (Sika Grout 200) with a medium thickness of 7 mm. A point to be noted is that the Sika Grout 200 was used to fill the voids between the impregnation layer and the slabs.

To simulate the loading of the vehicles on the road, a metal loading bogey, shown in Fig. 2, was used after making sure that the grout layer became hardened completely. Furthermore, the loading was carried out at a rate of 25 kN/min. In addition, the corresponding settlement values were read. Finally, all the previous operations were performed on each tested slab.

Table 2 Results of the tests performed on the sub-base samples

Test	First sample	Second sample	Third sample
Soil classification	(A-2–4)	(A-1-a)	(A-1-b)
Modified proctor	Maximum dry density (g/cm^3) = 2.146 Optimum moisture content = 7.1%	Maximum dry density (g/cm^3) = 2.107 Optimum moisture content = 7%	Maximum dry density (g/cm^3) = 2.052 Optimum moisture content = 7.2%
California bearing ratio (CBR)	20%	26%	23.9%

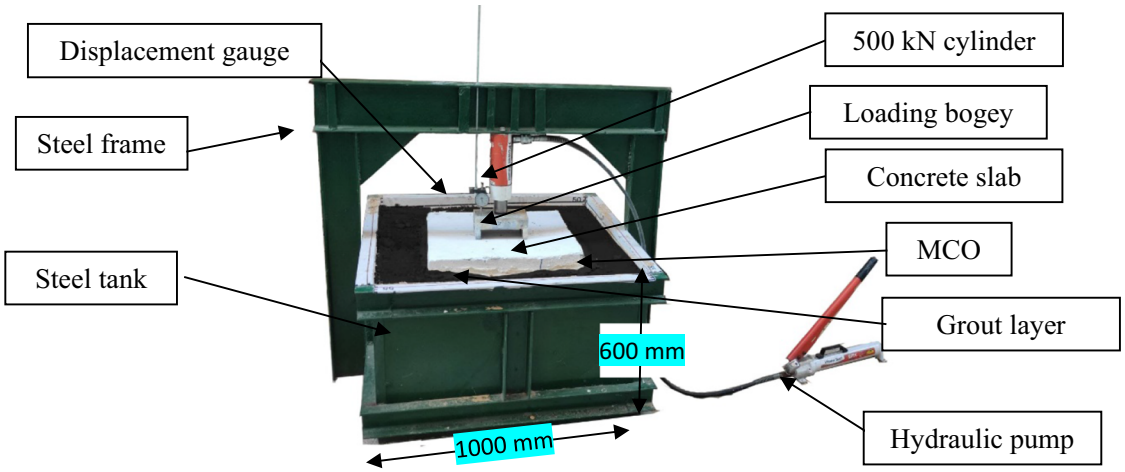

a- The shape of the test device

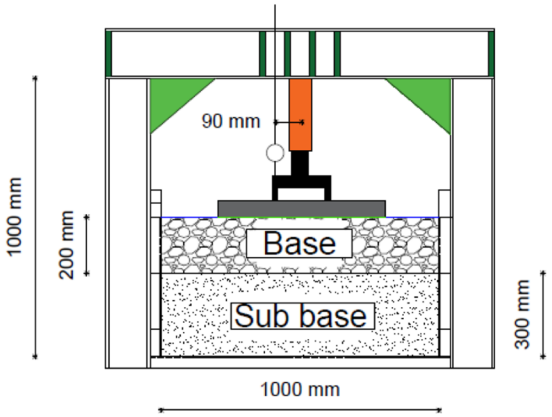

b- A section showing the dimensions and the components of the device

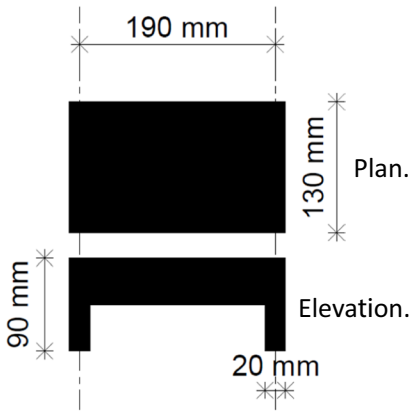

c- A section showing the dimensions of the loading plate (bogey)

Fig. 2 The components of the device used to perform the test

Experimental results

By conducting tests on different concrete slabs, it was found that there was a similarity in the pattern of the beginning of cracking for all slabs; the cracks started from the middle of the bottom of the slabs and went in a direction parallel to the long rib of the loading bogey. Moreover, the cracks started to occur in the transverse direction. It was observed that the cracks were dense (in a large number) in the slabs made of SHCC (Fig. 5e). However, the cracks were dense in an average number in the slabs made of HSC (Fig. 5c), while they are few in the slabs made of NSC (Fig. 5a). An important point to be noted is that this contrast in the cracks between the different slabs may be due to the ductile behavior of SHCC concrete when compared to other types of concrete used.

By studying the relationship between the load and the settlement for the different slabs (Fig. 3), it was found that the maximum bearing load of the slabs made of SHCC, HSC and NSC was 351.50, 306.50 and 198.90 kN, respectively. These results indicated that the slab made of SHCC was the slab with the maximum bearing capacity, followed by the HSC, and the NSC, respectively. Table 4 shows the amount of increase in the maximum load for each slab, when compared to the slabs made of NSC as a reference slab.

The initial stiffness can be defined as the slope of the linear segment at the beginning of the load–displacement curve, representing its resistance to deformation. The initial stiffness values for NSC, HSC and SHCC are 12.50, 20.82 and 21.90 kN/m, respectively. HSC shows an increase of approximately 66.56% in initial stiffness

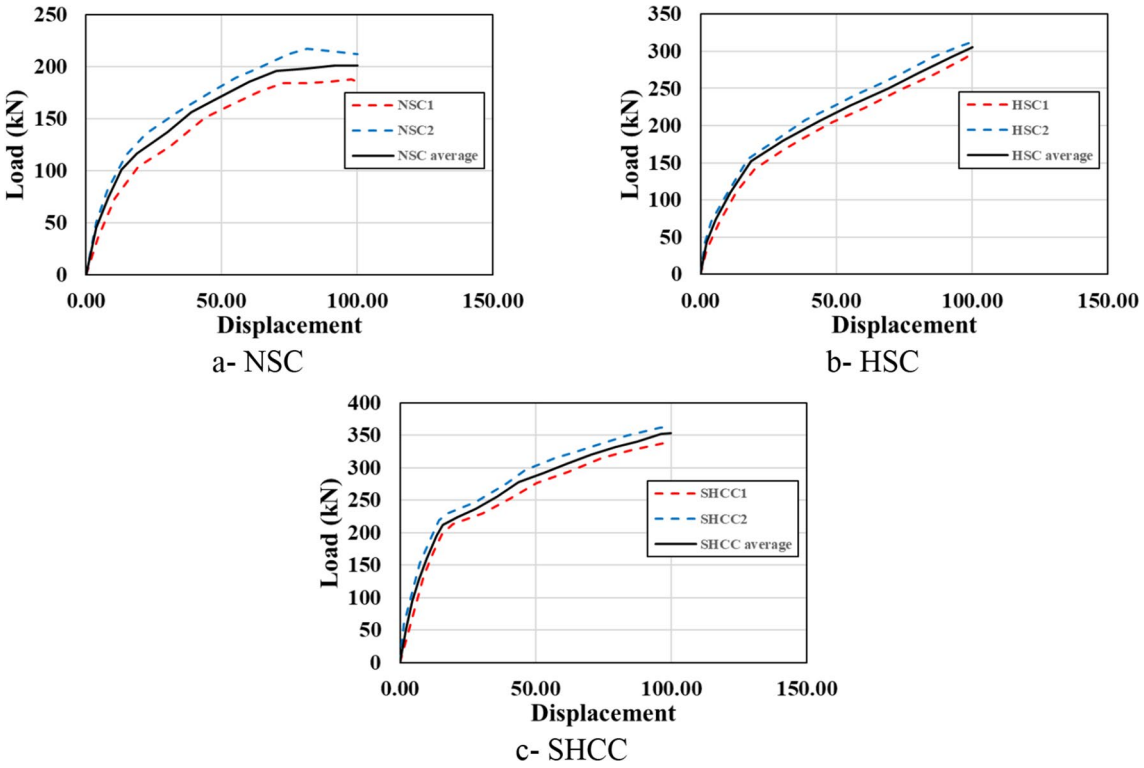

Fig. 3 The load–settlement curves for different slabs

Table 4 Percentage increase in the maximum load for the different slabs

Type	Average maximum load (kN)	% Of the increase in the maximum load	(K) Initial stiffness (kN/mm)	(T) Toughness (kN mm)	US dollar/kN
NSC	198.90	–	12.50	15,638	0.84
HSC	306.50	54	20.82	20,710	0.77
SHCC	351.50	76.6	21.90	26,876	0.95

compared to NSC. SHCC demonstrates a significant increase of approximately 75.20% in initial stiffness when compared to NSC.

Toughness can be defined as the area under the load–displacement curve, representing ductility. The toughness for NSC, HSC and SHCC, respectively, is 15,638, 20,710 and 26,876 kN mm. HSC exhibits an increase of approximately 32.43% in toughness compared to NSC. SHCC demonstrates a significant increase of approximately 71.86% in toughness when compared to NSC.

By calculating the cost of producing a cubic meter from SHCC, HSC and NSC when conducting the recent study, it was found to be equal to 335, 235 and 167 US dollars, respectively. Considering the cost required to increase the capacity of the pavement by one kilo Newton using each type of concrete, it can deduced that the most economical type was the HSC.

Numerical modeling

The numerical study of the current research was carried out based on the Abaqus program [37], which was based on the finite element method. Furthermore, the modeling was done using four parts: the first part was the loading bogey, the second part represented the concrete slab, the third part was the base and sub base layers, and finally, the fourth part represented the rigid tank. It is worth mentioning that the C3D8R element (An eight-node linear brick, reduced integration, hourglass control) was used for all parts except for the rigid tank, which was modeled as the S4R shell element

Table 5 Variables used in numerical modeling to model different types of concrete

Type	Elastic modulus E (N/mm^2)	Poisson ratio (ν)	Dilation angle (ψ)*	Eccentricity (ϵ)*	Shape parameter (K_c)*	(f_{bo}/f_{co})* Maximum compression axial/biaxial	Viscosity (μ)*
NSC	31,600	0.2	30°	0.1	0.667	1.16	0
HSC	55,000	0.2	30°				
SHCC	57,000	0.17	35°				

*Ψ is the dilation angle, measured in p-q plane and should be defined to calculate the inclination of the plastic flow potential in high confining pressures. The dilation angle is equal to the friction angle in low stresses. In higher level of confinement stress and plastic strain, dilation angle is decreased—Є is the flow potential eccentricity. It is a small positive number, which defines the range that the plastic potential function closes to the asymptote—K_c is the ratio of the second stress invariant in the tensile meridian to compressive meridian for any defined value of the pressure invariant at initial yield. It is used to define the multi-axial behavior of concrete—f_{b0}/f_{c0} is the proportion of initial equibiaxial compressive yield stress and initial uniaxial compressive yield stress—μ is the viscosity parameter; in comparison with characteristic time increment, it should be small

(A four-node doubly curved thin or thick shell, reduced integration, hourglass control, finite membrane strains). Moreover, the loading bogey was defined as an elastic element with an elastic modulus E = 200,000 N/mm^2 and Poisson's ratio equal to 0.3, while the CDP (concrete damage plasticity) model was used to represent the concrete in the nonlinear phase. The characteristics of this model are shown in Table 5. Carrira model [38] was used to model the compressive and tensile behavior of concrete.

A sensitivity analysis was conducted to adjust the numerical model for NSC, HSC and SHCC. The analysis focused on two key numerical parameters: mesh size in the thickness direction (l) and dilation angle (ψ). Each parameter underwent adjustments across a range of feasible values to assess its impact. Mesh sizes of 5, 10 and 15 mm were examined, with smaller mesh sizes yielding more accurate results. However, no substantial disparities were observed as the size increased from 5 to 10 mm. Therefore, a mesh size of 10 mm was chosen to optimize computational efficiency. Furthermore, dilation angles of 10°, 20°, 30° and 35° were selected. The numerical findings indicated that lower dilation angles exhibit a higher propensity for brittle behavior, leading to the failure of associated models due to concrete cracking, while higher dilation angles exhibit a more ductile behavior, resulting in failure due to concrete crushing, but exceeding ψ more 35° led to a slight underestimation of results. Ultimately, the most accurate predictions were achieved using a dilation angle of ψ = 30° for NSC and HSC, while ψ = 35° was ideal for SHCC. Other constitutive parameters for the CDP were defined following the recommended default values specified in the manual, which were 0.1 for Є, 1.16 for f_{bo}/f_{co}, 2/3 for K_c and 0 for μ. These default values indicated negligible deviations between the experimental and numerical results.

According to [39], the elastic behavior of the base and sub-base layers was modeled by setting $E = 20$ N/mm^2 and Poisson's ratio 0.3, while the Mohr–Coulomb plasticity model was used to model the inelastic behavior by placing friction angle = 40°, dilation angle = 0 and cohesion = 0.01 N/mm^2.

The interaction between the concrete slab and the loading plate, the concrete slab and the top surface of the base layer, and the surfaces of the tank adjacent to the two layers of the base and sub base was considered a hard contact interaction that allowed separation with penalty friction coefficient = 0.25. In addition, all the surfaces of the rigid tank were prohibited from moving in all directions. The analysis

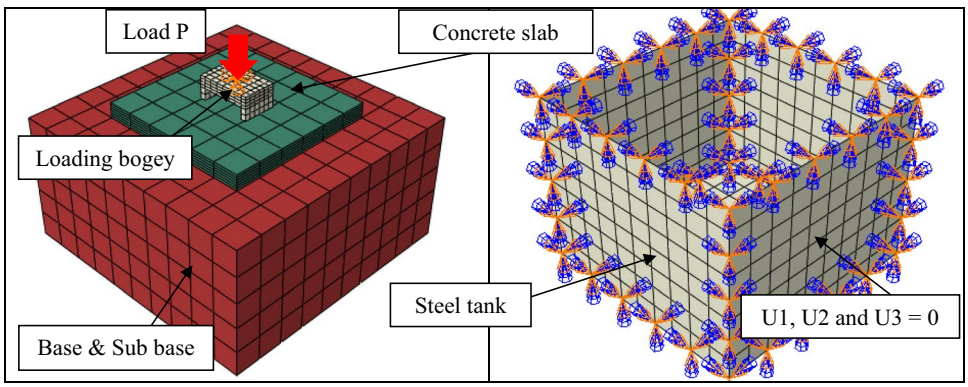

Fig. 4 Details of the numerical model

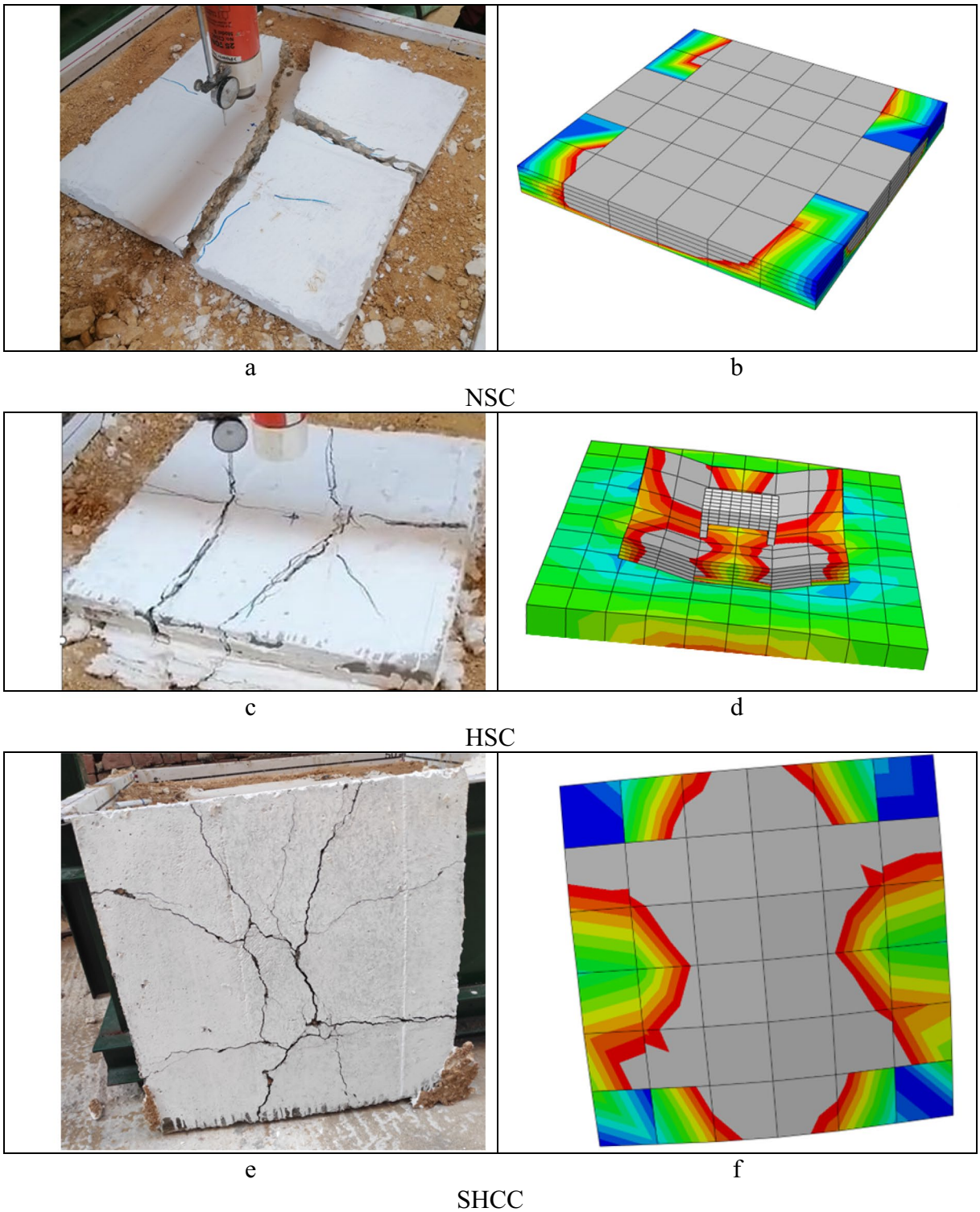

Fig. 5 Comparison of experimental and numerical collapse patterns for different slabs

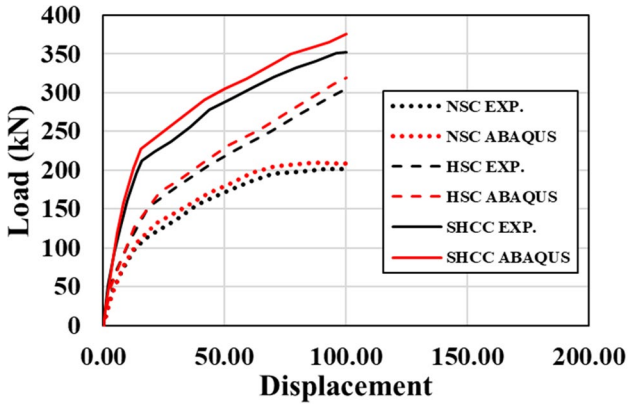

Fig. 6 Comparison of the numerical and experimental load–settlement curves for the tested slabs

was carried out with a load in a place similar to the hydraulic cylinder loading point above the loading plate. Figure 4 shows the details of the numerical model.

Figure 5 shows a comparison between the experimental and the numerical collapse patterns. According to Fig. 5, it is clear that the numerical modeling succeeded in modeling the behavior of the tested slabs.

Figure 6 shows a comparison between the load–settlement curves for all the slabs experimentally and numerically. According to Fig. 6, it can be deduced that there was a great agreement in the behavior of all the tested slabs.

Figure 7 shows the profile of the vertical displacement of the different slabs along the two paths of the slab passing through the center during loading, at displacements of 20, 40, 60, 80 and 100 mm. An important point to be noted is that the slab made of NSC suffered from positive displacements at its end (raised from the base layer) in the direction parallel to the short length of the bogey (see Fig. 7a). Such a behavior was due to the relatively low elasticity and the tensile strength of this type of concrete.

Figure 8 shows the comparison of the vertical displacement profile of the different slabs at a displacement of 100 mm. It shows the ability of the SHCC slabs to distribute stresses on the surface of the base layer when compared to the slabs made of NSC or HSC. Such an ability of the SHCC slabs was due to the fact that the vertical displacement of the edge of the slab, which was in the direction of the long length of the bogey, had not been less than 75% of its center displacement (see Fig. 7b).

Conclusion

This research conducts an experimental and numerical investigation into the performance of rigid pavement constructed from various concrete types under static load conditions. The recent experimental study involves six slabs, each measuring $600 \times 600 \times 60$ mm, and they are made from different types of concrete, including normal-strength concrete (NSC), high-strength concrete (HSC) and strain hardening cementitious composites (SHCC). According to the current research, it can be concluded that:

1- By using the concrete pavement made from SHCC, it was found that the bearing capacity of the pavement increased by 76.6%, compared to NSC pavement.
2- The bearing capacity of the HSC pavement increased by 54%, compared to NSC pavement. Moreover, the maximum load for the slabs made from SHCC, HSC and NSC could bear 351.50, 306.50 and 198.90 kN, respectively. Regarding the cost required to increase the capacity of the pavement by one kilo Newton using each type of concrete, it can be deduced that HSC is the most cost-effective option.
3- The initial stiffness values are 12.50 kN/m for NSC, 20.82 kN/m for HSC and 21.90 kN/m for SHCC. HSC exhibits an approximately 66.56% increase in initial stiffness compared to NSC, while SHCC demonstrates a significant increase of around 75.20% compared to NSC.
4- The toughness values are 15,638 kN mm for NSC, 20,710 kN mm for HSC and 26,876 kN mm for SHCC. HSC exhibits an approximate 32.43% increase in toughness compared to NSC, while SHCC demonstrates a substantial increase of approximately 71.86% in toughness when compared to NSC.
5- The numerical study succeeded in modeling the nonlinear behavior of different types of pavements, in which different types of concrete were used.
6- It was deduced that the SHCC pavement was able to distribute stresses better than the NSC and the HSC pavements, due to its modulus of elasticity, high tensile strength and ability to distribute cracks.

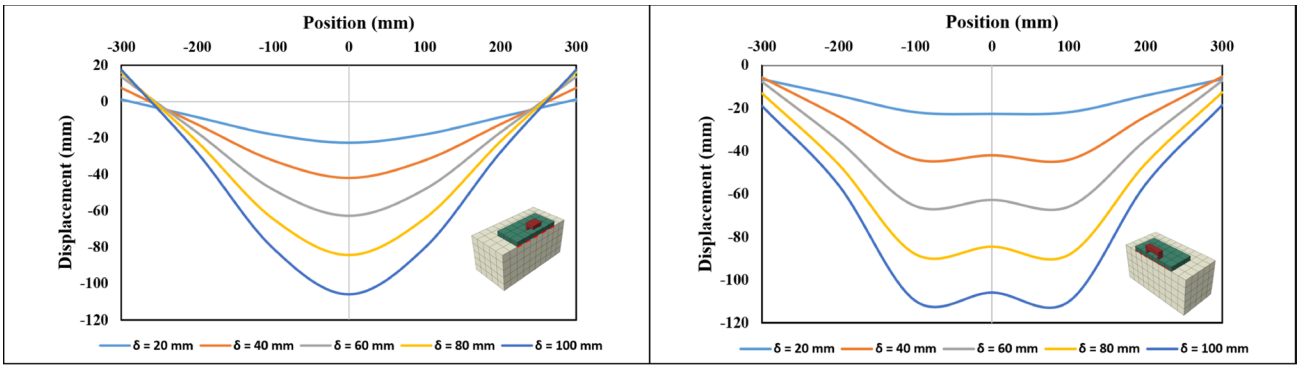

a b

NSC

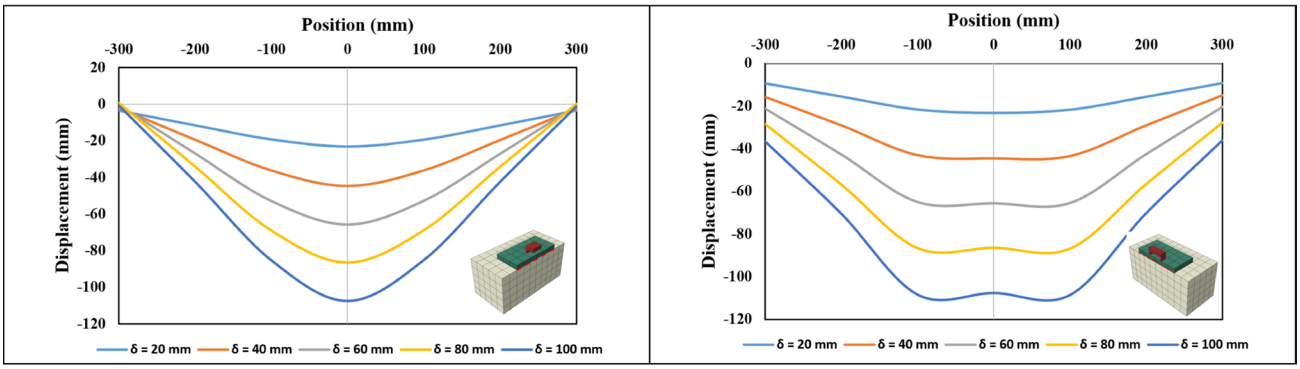

c d

HSC

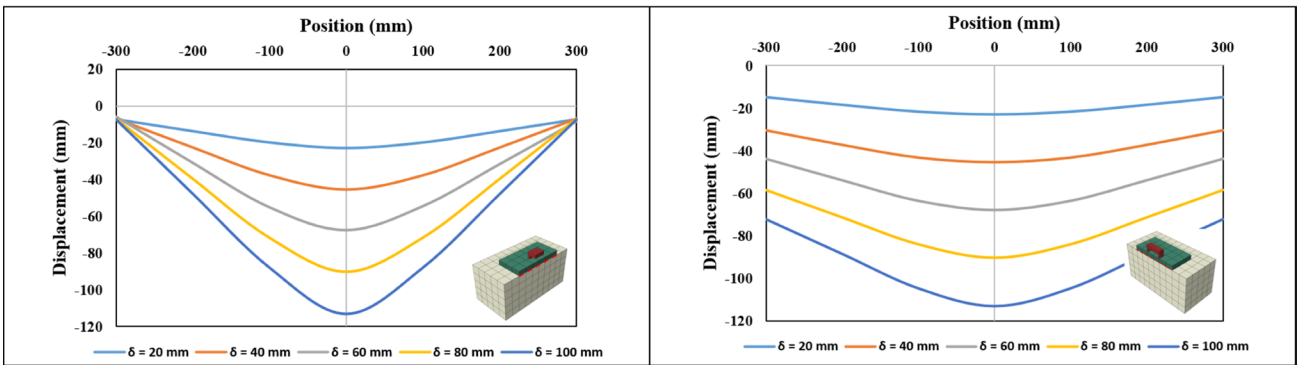

e f

SHCC

Fig. 7 Displacements along the axes of the slabs in the short and long length directions of the bogey

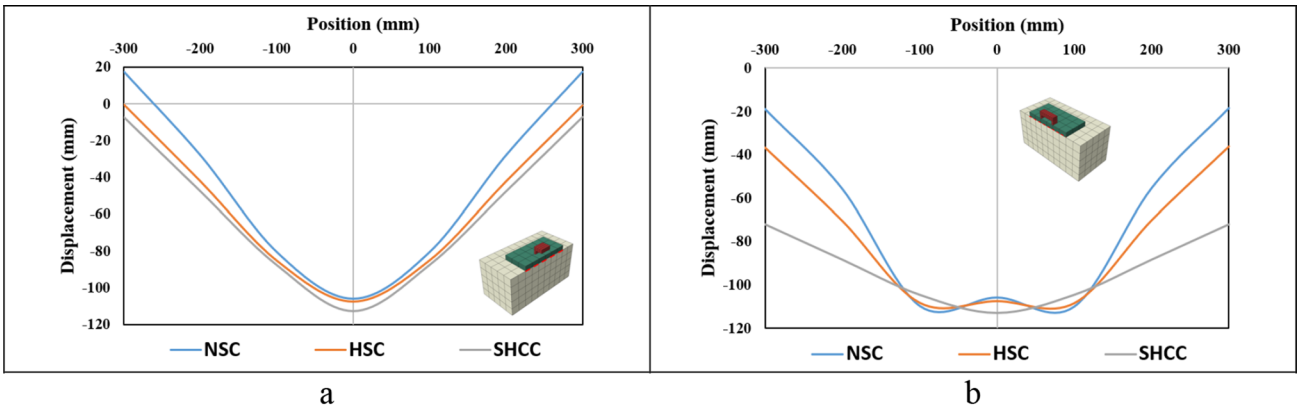

Fig. 8 Vertical displacements of different slabs along the two paths of the center of the slab at δ = 100 mm

Funding Open access funding provided by The Science, Technology & Innovation Funding Authority (STDF) in cooperation with The Egyptian Knowledge Bank (EKB).

Declarations

Conflict of interest The authors declare no conflict of interest.

Ethical approval This article does not contain any studies with human participants or animals performed by any of the authors.

Informed consent For this type of study formal consent is not required.

References

1. Hajj EY, Sebaaly PE, Kandiah P (2010) Evaluation of the use of reclaimed asphalt pavement in airfield HMA pavements. J Transp Eng 136(3):181–189
2. Topini D, Toraldo E, Andena L, Mariani E (2018) Use of recycled fillers in bituminous mixtures for road pavements. Constr Build Mater 159:189–197
3. Speight JG (2016) Asphalt materials science and technology. Butterworth-Heinemann is, pp 437–474
4. Aatheesan TBMWJA, Arulrajah A, Bo MW, Vuong B, Wilson J (2010) Crushed brick blends with crushed rock for pavement systems. In: Proceedings of the institution of civil engineers-waste and resource management. Thomas Telford Ltd, vol 163, no 1, pp 29–35
5. Gupta A (2004) Report on case studies on failure of bituminous pavements report submitted to PWD. Aligarh, pp 1–14.
6. Gong M, Xiong Z, Chen H, Deng C, Chen X, Yang J (2019) Evaluation on the cracking resistance of semi-flexible pavement mixture by laboratory research and field validation. Constr Build Mater 207:387–395
7. Zhang Y, Wu DQ (2020) General applications of the semi-rigid pavement in South East Asia. Int J Pavement Res Technol 13(3):296–302
8. Pranav S, Aggarwal S, Yang EH, Sarkar AK, Singh AP, Lahoti M (2020) Alternative materials for wearing course of concrete pavements: a critical review. Constr Build Mater 236:117609
9. Shill SK, Al-Deen S, Ashraf M, Rashed MG, Hutchison W (2022) Consequences of aircraft operating conditions at military airbases: degradation of ordinary mortar and resistance mechanism of acrylic and silica fume modified cement mortar. Road Mater Pavement Des 23(1):98–111
10. Cabalar AF, Zardikawi OAA, Abdulnafaa MD (2019) Utilisation of construction and demolition materials with clay for road pavement subgrade. Road Mater Pavement Des 20(3):702–714
11. Highways Agency (1994) Design manual for roads and bridges. HM Stationery Office
12. Gautam PK, Kalla P, Jethoo AS, Agrawal R, Singh H (2018) Sustainable use of waste in flexible pavement: a review. Constr Build Mater 180:239–253
13. Kolesnikov A, Tolmacheva T (2019) Ways to minimize volume (weight) and increase the bearing capacity of rigid pavement. Civ Eng J 5(11):2495–2501
14. Busari A, Dahunsi B, Akinmusuru J (2019) Sustainable concrete for rigid pavement construction using de-hydroxylated Kaolinitic clay: Mechanical and microstructural properties. Constr Build Mater 211:408–415
15. Zhang H (1999) Semi-flexible pavement with cement mortar mix design. Jilin Highway Transp Res 2:8–23
16. Ayobami B, Julius N, Emmanuel S, Snyman J, Williams K, Olugbenga A, Loto RT (2021) Permeable pavements for storm water control incorporating nano clay. Cogent Eng 8(1):1817254
17. Dong Q, Zhao X, Chen X, Ma X, Cui X (2021) Long-term mechanical properties of in situ semi-rigid base materials. Road Mater Pavement Des 22(7):1692–1707
18. Nawir D, Mansur AZ (2022) Effects of HDPE utilization and addition of wetfix-be to asphalt pavement in tropical climates. Civ Eng J 8(8):1665–1678
19. Nistratov AV, Klimenko NN, Pustynnikov IV, Vu LK (2022) Thermal regeneration and reuse of carbon and glass fibers from waste composites. Emerg Sci J 6:967–984

20. Junaid M, Shah MZA, Yaseen G, Awan HH, Khan D, Jawad M (2022) Investigating the effect of gradation, temperature and loading duration on the resilient modulus of asphalt concrete. Civ Eng J 8(02)
21. Rout MD, Biswas S, Shubham K, Sinha AK (2023) A systematic review on performance of reclaimed asphalt pavement (RAP) as sustainable material in rigid pavement construction: Current status to future perspective. J Build Eng 76:107253
22. Zhao Z, Xu L, Li X, Guan X, Xiao F (2023) Comparative analysis of pavement performance characteristics of flexible, semi-flexible and rigid pavement based on accelerated pavement tester. Constr Build Mater 387:131672
23. Ariyanti D, Sasongko NA, Fansuri MH, Fitriana EL, Nugroho RA, Pratiwi SA (2023) Retrofitting of concrete for rigid pavement using bacterial: a meta-analysis. Sci Total Environ 166019
24. Wang C, Xiao W, Liu J (2023) Developing an improved extreme gradient boosting model for predicting the international roughness index of rigid pavement. Constr Build Mater 408:133523
25. Karikatti V, Chitawadagi MV, Devarangadi M, Sanjith J, Reddy NG (2023) Influence of bagasse ash powder and marble powder on strength and microstructure characteristics of alkali activated slag concrete cured at room temperature for rigid pavement application. Cleaner Mater 9:100200
26. Somani P, Gaur A (2023) Temperature sensitivity analysis on mechanical properties of phase changing material incorporated rigid pavement. Mater Tod
27. Pal R, Sarkar PP (2023) Developing a model of porous concrete-filled rigid pavement. Mater Today Proc
28. Kumar S, Sharma U (2023) Comparative analysis between use of waste glass in rigid pavement and alkali resistant glass fibers for use in paver blocks. Mater Today Proc
29. Mohammad I, Rana AS (2023) Incorporation of phosphogypsum with cement in rigid pavement: an approach towards sustainable development. Mater Today Proc
30. Cho YH, Liu C, Dossey T, McCullough BF (1998) Asphalt overlay design methods for rigid pavements considering rutting, reflection cracking, and fatigue cracking. Research report September 1996–August 1997 (No. PB-99–123994/XAB; CTR-987–9). Texas Univ., Center for Transportation Research, Austin, TX (United States); Texas Dept. of Transportation, Austin, TX (United States)
31. Croney D, Croney P (1991) The design and performance of road pavements.
32. Swaddiwudhipong S, Lu HR, Wee TH (2003) Direct tension test and tensile strain capacity of concrete at early age. Cem Concr Res 33(12):2077–2084
33. Tahir MFM, Abdullah MMAB, Abd Rahim SZ, Hasan MRM, Saafi M, Jaya RP, Mohamed R (2022) Potential of industrial by-products based geopolymer for rigid concrete pavement application. Constr Build Mater 344:128190
34. Elsamak G, Abdullah A, Salama MI, Hu JW, El-Mandouh MA (2022) Punching shear behavior of slabs made from different types of concrete internally reinforced with SHCC-filled steel tubes. Materials 16(1):72
35. Zeng JJ, Zeng WB, Ye YY, Liao J, Zhuge Y, Fan TH (2022) Flexural behavior of FRP grid reinforced ultra-high-performance concrete composite plates with different types of fibers. Eng Struct 272:115020
36. AASHTO M 145-91 (2012) Classification of soils and soil-aggregate mixtures for highway construction purposes
37. Hibbitt, Karlsson, and Sorensen, Inc. ABAQUS Theory manual, User manual and Example Manual, Version 6.7. Providence, RI; 2000
38. Carreira DJ, Chu KH (1985) Stress-strain relationship for plain concrete in compression. J Proc 82(6):797–804
39. Bhasi A, Rajagopal K (2015) Geosynthetic-reinforced piled embankments: comparison of numerical and analytical methods. Int J Geomech 15(5):04014074